Carbohydrate Polymers 136 (2016) 71–80

Contents lists available at ScienceDirect

Carbohydrate Polymers

journal homepage: www.elsevier.com/locate/carbpol

Alginate stabilized gold nanoparticle as multidrug carrier: Evaluation of cellular interactions and hemolytic potential

Soma Dey [a], M. Caroline Diana Sherly [b], M.R. Rekha [b], K. Sreenivasan [a,*]

[a] Laboratory for Polymer Analysis, Biomedical Technology Wing, Sree Chitra Tirunal Institute for Medical Sciences and Technology, Poojapura, Trivandrum 695012, India
[b] Division of Biosurface Technology, Biomedical Technology Wing, Sree Chitra Tirunal Institute for Medical Sciences and Technology, Poojappura, Trivandrum 695012, Kerala, India

ARTICLE INFO

Article history:
Received 2 March 2015
Received in revised form 27 August 2015
Accepted 7 September 2015
Available online 9 September 2015

Keywords:
Curcumin
Alginate
Polymer–drug conjugates
Methotrexate
Gold nanoparticles
Confocal laser scanning microscopy

ABSTRACT

This work delineates the synthesis of curcumin (Ccm) and methotrexate (MTX) conjugated biopolymer stabilized AuNPs (MP@Alg–Ccm AuNPs). The dual drug conjugated nano-vector was characterized by FTIR, ^{1}H NMR and UV–vis spectroscopic techniques. Hydrodynamic diameter and surface charge of the AuNPs were determined by DLS analysis and the spherical particles were visualized by TEM. MP@Alg–Ccm AuNPs exhibited improved cytotoxic potential against C6 glioma and MCF-7 cancer cell lines and was found to be highly hemocompatible. MP@Alg–Ccm AuNPs also exhibited active targeting efficiency against MCF-7 cancer cells due to the presence of "antifolate" drug MTX. Thus MP@Alg–Ccm AuNPs may find potential application in targeted combination chemotherapy for the treatment of cancer. The study is also interesting from the synthetic point of view because, here generation of AuNPs was done using "green chemical" alginate and dual drug conjugated AuNPs were created in two simple reaction steps using "green solvent" water.

1. Introduction

Curcumin (Ccm) is a polyphenolic compound extracted from the rhizome of the plant *Curcuma longa* (Indian spice turmeric). Within the last couple of decades, extensive research work has unveiled a wide range of striking pharmacological activities in Ccm such as antioxidant, anti-inflammatory, antiproliferative and antiangiogenic activities (Aggarwal, Kumar, & Bharti, 2003; Aggarwal & Sung, 2009; Lantz, Chen, Solyom, Jolad, & Timmermann, 2005; Motterlini, Foresti, Bassi, & Green, 2000; Shi et al., 2006). It has been reported that the transcriptional nuclear factor kappa beta (NFκβ) is the chief controller of cell proliferation, inflammation, apoptosis and resistance in cells and Ccm inhibits NF-κβ resulting in blockage of the function of protein kinase C, receptor tyrosine kinase, Her-2 and epidermal growth factor to induce apoptosis. Most interestingly, development of resistance to Ccm is less likely as it induces apoptosis through multiple cell signaling pathways (Ravindran, Prasad, & Aggarwal, 2009). In cancer therapy Ccm can exhibit pleiotropic therapeutic effect because of its ability to inhibit multiple levels of diverse cell signaling pathways (Maher et al., 2011). Moreover, Ccm can also down regulate the levels of Pgp, ABCG2 and MRP-1 (three major ABC drug transporters that are mainly responsible for the development of multi drug resistance [MDR] in cancer cells) and thus it has significant role in controlling MDR (Misra & Sahoo, 2011). However, Application of Ccm as a chemotherapeutic agent is restricted due to its extremely low aqueous solubility, instability and consequent poor bioavailability (Anand, Kunnumakkara, Newman, & Aggarwal, 2007). In order to redress these problems, several approaches have been proposed and among them conjugation of Ccm to hydrophilic polymers is a wise approach. Conjugation of hydrophobic drugs to suitable polymers augments aqueous solubility of the drug, ensures unhindered release and offers a chance to alter drug pharmacokinetics and biodistribution which are basically useful for those drugs that exhibit rapid metabolism (e.g. curcumin), faster clearance and/or off target toxicities (anticancer drugs) (Larson & Ghandehari, 2012). It has been reported that Ccm can boost the antitumor efficiency of several chemotherapeutic agents like paclitaxel and doxorubicin (Duan et al., 2012; Ganta & Amiji, 2009; Manju, Sharma, & Sreenivasan, 2011). A recent report suggests that curcumin can significantly enhance the uptake and cytotoxicity of methotrexate (MTX) in KG-1 leukemic cells (Dhanasekaran, Biswal, Sumantran, & Verma, 2013).

MTX, an antimetabolite, is structurally analogous to folic acid (FA). The difference in structure between FA and MTX is due to

* Corresponding author.
E-mail address: sreeni@sctimst.ac.in (K. Sreenivasan).

http://dx.doi.org/10.1016/j.carbpol.2015.09.016
0144-8617/

the functional group at 4th position of pteridine ring (FA has —OH and MTX has —NH_2 group). This structural feature of MTX allows it to bind tightly to dihydrofolate reductase (DHFR) which is a vital enzyme in folic acid cycle catalyzing the conversion of dihydrofolate to active tetrahydrofolate. Thus MTX interrupts DNA and RNA synthesis by inhibiting DHFR and induces cellular apoptosis. Hence the antifolate drug can play the role of a chemotherapeutic agent. In addition to this, being a FA analog MTX has been established to be an efficient ligand for active targeting (Dhar, Liu, Thomale, Dai, & Lippard, 2008; Kohler, Sun, Wang, & Zhang, 2005). The main drawback associated with MTX is its cellular efflux and consequent resistance to the drug developed in the targeted cells. In order to offset this fact, MTX conjugates with suitable polymers such as poly(ethyleneglycol), hyaluronic acid and poly (glutamic acid) have been developed (Piper, McCaleb, & Montgomery, 1983; Riebeseel et al., 2002).

The conventional drug delivery systems (DDS) possess several limitations like poor bioavailability, non-specific biodistribution, lack of targeting, side effects and low therapeutic indices. Nanotherapeutics has the potential to surmount these limitations to a large extent (Malam, Loizidou, & Seifalian, 2009; Moorthi, Manavalan, & Kathiresan, 2011). Among various nanotherapeutics, gold nanoparticles (AuNPs) have been widely used as the potential drug delivery vehicle (Boisselier & Astruc, 2009). Facile synthetic procedure, convenient surface modification, excellent stability and low cytotoxicity are some of the distinctive attributes which have made AuNPs a subject of intense research (Daniel & Astruc, 2004; Giljohann et al., 2010). Polymeric nanoparticles (micelles, vesicles), liposomes are also widely studied for delivery of hydrophobic drugs. Compared to those nanoparticles, functionalized AuNPs with much smaller size are advantageous for passive tumor targeting *via* enhanced permeation and retention (EPR) effect along with reduced clearance through reticuloendothelial system (RES) (Gref et al., 1994; Maeda, Wu, Sawa, Matsumura, & Hori, 2000). Thus AuNPs functionalized with suitable targeting ligands can serve as excellent vehicles for hydrophobic drugs and other bioactive agents with augmented longevity in blood stream and improved uptake by cells due to both EPR effect and targeting ligand mediated endocytosis (Manju & Sreenivasan, 2012). However, in most of the cases AuNPs containing manifold functionalities (*e.g.*, various drugs and targeting ligands) are developed following multiple synthetic steps and using hazardous organic solvents. Often rigorous purification steps are employed in designing such type of AuNPs based nano-vectors. All these can have adverse effect on the stability of the nano-vectors.

Herein we report the fabrication of a double drug containing biopolymer stabilized AuNPs *via* green synthetic route and following only two simple reaction steps. Recently we developed alginate–curcumin (Alg–Ccm) conjugate (Dey & Sreenivasan, 2014) in our laboratory. The study showed that Alg–Ccm enhances aqueous solubility, stability and therapeutic efficacy of Ccm. In the present study we simultaneously generated and stabilized AuNPs using the Alg–Ccm conjugate in aqueous medium under thermal activation. Here we hypothesized that alginate possessing secondary hydroxyl groups can reduce Au(III) to Au(0). Besides, the structure of alginate being oxygen rich, it can effectively cap the new born AuNPs and protect them from aggregation. With an aim to redress the efflux of MTX from cancer cells, we covalently conjugated MTX to bis(aminopropyl) terminated poly(ethylene glycol) in aqueous buffer solution (of pH 7.4) to get MP conjugate which was subsequently conjugated onto the Alg–Ccm AuNPs in aqueous medium to get the hybrid nano-structured DDS MP@Alg–Ccm AuNPs. Alginate, present in brown algae and bacteria, is considered as a "green chemical" (Yang, Ren, & Xie, 2011). The entire synthetic work was done using "green solvent" water and double drug conjugated biopolymer stabilized AuNPs were designed through two facile reaction steps. The cytotoxic potential of the dual drug conjugated DDS was evaluated against C6 glioma (from rat brain tumor) and MCF-7 (human breast cancer) cells. Facile uptake of MP@Alg–Ccm AuNPs by the cancer cell lines was confirmed by both fluorescence microscopic and confocal laser scanning microscopic imaging. Percentage of hemolysis caused by the DDS was also studied to assess the blood compatibility of the DDS.

2. Experimental

2.1. Materials

Tetrachloroauric acid(III) trihydrate ($HAuCl_4{\cdot}3H_2O$), 1,3-dicyclohexylcarbodiimide (DCC), 4-dimethylaminopyridine (DMAP), N-(3-dimethylaminopropyl)-N-ethylcarbodiimide hydrochloride (EDC), N-hydroxysuccinimide (NHS), Bis (aminopropyl) terminated polyethyleneglycol (Bis(aminopropyl) terminated PEG), Methotrexate hydrate (MTX) were purchased from Sigma–Aldrich (Bangalore, India). Curcumin (95% total curcuminoid content) from turmeric rhizome was obtained from Alfa Aesar (Bangalore, India). Sodium alginate was purchased from SD fine chemicals (Mumbai, India). The average molecular weight of Sodium alginate used in this study was found to be 4×10^5 g/mol by GPC analysis. Sodium poly(guluronate) (G-block) was isolated according to the procedure by Bouhadir, Hausman and Mooney (1999) (the procedure is mentioned in brief in Supplementary Information). GPC analysis of the G-block resulted in polymer with significantly lower molecular weight of 10,281 g/mol. The molecular weight of guluronic acid and mannuronic acid in its deprotonated form ($C_6H_7O_6$) is 176.1 g/mol. Hence there are almost (10,281/176.1) 58 units of guluronic acids in the G-block polymer isolated from sodium alginate.

Dimethyl sulfoxide (DMSO) and ethanol (EtOH) were obtained from Merck (Mumbai, India). Ultra pure water (18.2 mΩ resistivity) was obtained from a Mili-Q water purification system. Deionized water was used all through the reaction and purification steps in this study.

C6 (Glial cells from rat Glioma) and MCF-7 (human breast cancer cells) cell lines were obtained from the National Centre for Cell Sciences (NCCS), Pune, India. 3-(4,5-Dimethylthiazol-2-yl)-2,5-diphenyl tetrazolium bromide (MTT reagent), fetal bovine serum (FBS), minimum essential medium (MEM), Dulbecco's Modified Eagle's Medium (DMEM)/Nutrient F-12 Ham and Trypsin/EDTA were purchased from Sigma-Aldrich (Bangalore, India). RPMI 1640 medium, Hoechst 33342 and Fluorescence isothiocyanate (FITC) were purchased from Invitrogen (Bangalore, India).

2.2. Synthesis of Alg–Ccm conjugate and generation of Alg–Ccm AuNPs

The Alg–Ccm conjugate was prepared according to our previous report (Dey & Sreenivasan, 2014). In brief, hydrophobic drug curcumin was directly covalently conjugated to the C-6 carboxylate functional group of biopolymer alginate *via* esterification reaction using DCC/DMAP in H_2O-DMSO medium. The conjugate was purified by dialysis (using a dialysis membrane of MWCO 3500) against DMSO for one day and against H_2O for three days to remove any unreacted molecules. Alg–Ccm conjugate was lyophilized and stored in the refrigerator for further applications.

AuNPs were generated and stabilized by the Alg–Ccm conjugate in aqueous medium under thermal activation. An aqueous solution of $HAuCl_4$, $3H_2O$ (1 mM) was slowly added to the aqueous solution of Alg–Ccm conjugate (0.41 mg/mL) to maintain a final concentration of 10^{-2} M of chloroauric acid in the solution. After proper mixing the solution was heated gradually in a water bath and the

generation of AuNPs was indicated by a color change of the solution from yellow to pinkish red. The AuNPs solution was cooled to room temperature and dialyzed against deionized water (using a dialysis membrane of MWCO 3500) for 1 day. Finally the solution was lyophilized and stored in refrigerator.

2.3. Synthesis of MTX conjugated Alg–Ccm AuNPs (MP@Alg–Ccm AuNPs)

In order to develop MTX conjugated Alg–Ccm AuNPs, at first MTX was conjugated to Bis (aminopropyl) PEG to generate MTX–PEG conjugate (MP conjugate). For MP conjugate synthesis, MTX was dissolved in PBS (pH 7.4) and was activated using EDC and NHS (MTX:EDC:NHS = 1:1.3:1.1 molar ratio) at room temperature for one hour under the blanket of N_2 (g) in dark. Then solution of bis(aminopropyl) PEG (MTX:PEG = 1:1 molar ratio) in PBS (pH 7.4) was gradually added to the activated MTX solution and the mixture was allowed to stir at room temperature for around four hours in dark. Next, the MP conjugate was dialyzed (using dialysis membrane of MWCO 1000) against PBS (pH 7.4) for one day and against distilled H_2O for one day and was dried by lyophilization.

In the second step, MP conjugate was conjugated to the Alg–Ccm AuNPs utilizing the EDC chemistry. The free carboxyl functionality on Alg–Ccm AuNPs (15 mg) was activated with EDC/NHS (in aqueous carbonate/bicarbonate buffer medium with pH 8.2) for one hour at 25 °C followed by the addition of aqueous solution of MP conjugate (25 mg) and the reaction mixture was moderately stirred overnight at 25 °C. The reaction mixture was then dialyzed (MWCO 3500) and lyophilized to get MP@Alg–Ccm AuNPs.

2.4. Physicochemical characterizations of Alg–Ccm AuNPs and MP@Alg–Ccm AuNPs

The generation and stabilization of AuNPs using Alg–Ccm conjugate and its functionalization with MP conjugate to produce MP@Alg–Ccm AuNPs were characterized by analyzing the surface plasmon resonance (SPR) absorption spectra of the respective AuNPs using Ultraviolet–Visible (UV–Vis) spectrophotometer (Carry model 100 bio UV–Vis spectrophotometer, Melbourne, Australia). Generation of Alg–Ccm AuNPs was verified by comparing its X-ray diffraction pattern (Bruker D8 Advance; equipped with Cu Kα radiation source) with that of Alg–Ccm conjugate. The Fourier transform infrared spectra were recorded using a Nicolet 5700 FTIR spectrometer in the range of 4000–500 cm^{-1} after each step of modification. ^1H NMR spectra of Alg–Ccm AuNPs and MP@Alg–Ccm AuNPs were analyzed by 500 MHz spectrometer (Brucker Avance DPX 500) using D_2O as the solvent. The hydrodynamic diameter of the AuNPs was determined by dynamic light scattering instrument (DLS, Malvern Zetasizer Nano ZS, UK) with a He–Ne laser beam at a wavelength of 633.8 nm. To get an idea about the stability of the functionalized AuNPs, zeta potential (ξ, at 25° C and pH 7.4) was determined using the same instrument. The spherical morphology of the AuNPs was visualized by Transmission Electron microscopy (TEM; Hitachi H-7650; Tokyo, Japan). Sample for TEM analysis was prepared by depositing a drop of nanoparticle suspension on a 200 mesh copper TEM grid with formvar film and air dried at room temperature.

2.5. Determination of drug content in MP@Alg–Ccm AuNPs

The total MTX content in MP@Alg–Ccm AuNPs was determined by UV–vis spectroscopy (at λ_{max} = 369 nm) in PBS (pH 7.4). In order to determine the total Ccm content in MP@Alg–Ccm AuNPs, a known amount of fridge-dried sample was dispersed in EtOH and incubated for 24 h (at 37 °C and 120 rpm). After that the dispersion was centrifuged (at 14,000 rpm for 15 min) and the supernatant was collected. Using this supernatant solution, total Ccm content was determined by UV–vis spectroscopy (at λ_{max} = 428 nm).

2.6. Evaluation of cytotoxicity

The quantitative cytotoxic potential of MP@Alg–Ccm AuNPs was determined using two cancer cell lines: (i) C6 cancer cell and (ii) MCF-7 cancer cells. For the study against C6 cells, cells were maintained in 50:50 mixture of Dulbecco's Modified Eagle's Medium/Nutrient F-12 Ham and MEM supplemented with 10% FBS. Then 80% confluent cells were trypsinized and seeded in 96 well plates (1×10^3 cells/well) and incubated for 24 h. Then the cells were exposed to a series of doses of MP@Alg–Ccm AuNPs, free MTX and free Ccm in a CO_2 (5%) incubator at 37 °C. After 24 h incubation, the medium containing sample and free drug was removed from respective wells and 200 μL of freshly prepared MTT solution (0.5 mg/mL) in culture medium was added into each well. After 4 h incubation, MTT solution was carefully removed. DMSO (200 μL) was then added into each well and the plate was gently shaken for 10 min at room temperature to dissolve all precipitates formed. The absorbance of individual wells at 570 nm was then detected by a microplate reader (Tecan Infinite M200, Switzerland). Cell viability was expressed as the mean percentage of sample absorbance relative to untreated cells (control) as shown in the equation below (where *As* is the absorbance of sample and *Ac* is the absorbance of control). Here each reported value is the mean of three replicates.

$$\text{Cell viability}\,(\%) = \frac{As}{Ac} \times 100$$

For the study with MCF-7 cells, the cells were maintained in RPMI Medium. Then 80% confluent cells were trypsinized and seeded in 96 well plates (1×10^3 cells/well) and incubated for 24 h. Then similar procedure was adopted as described for C6 cell lines.

2.7. Cellular uptake study

Cellular images were acquired with a fluorescence microscope (Leica DM IRB, Germany) using C6 and MCF-7 cell lines. Cells were seeded and incubated on a 4-well plate at 37 °C for 24 h. Then both C6 and MCF-7 cells were exposed to FITC tagged MP@Alg–Ccm AuNPs. After incubation for 2.5 h, Hoechst 33342 solution (15 μL of concentration 10 μM) was added to each well for staining the nucleus. Then, after 30 min of incubation, the medium containing AuNPs sample and Hoechst was removed from each well and the cells were washed with PBS (twice) to remove any non-specific binding. After fixing the cells, uptake was detected in fluorescence microscope.

In order to confirm the targeting efficiency of MTX, FITC was tagged at the same density on MP@Alg–Ccm AuNPs and Alg–Ccm AuNPs. MCF-7 cells were treated with same concentration of FITC labeled MP@Alg–Ccm AuNPs and FITC labeled Alg–Ccm AuNPs. The cellular uptake in each case was studied following the same procedure as mentioned above.

Cellular uptake in both C6 glioma and MCF-7 cell lines was confirmed by confocal laser scanning microscopic images recorded in Nicon A1R.

2.8. Evaluation of hemolytic toxicity

The hemolytic toxicity of MP@Alg–Ccm AuNPs was determined by evaluating the percentage of hemolysis. Blood was drawn from a healthy unmedicated human donor and collected in anticoagulant ACD. MP@Alg–Ccm AuNPs was placed in polystyrene culture plates and agitated with PBS before they are exposed to blood. To each plate 10 mL blood was added (to maintain sample concentration of 0.5 mg/mL). 5 mL blood was immediately taken for initial analysis

and remaining 5 mL blood (with sample) was incubated for 30 min under agitation at 70 ± 5 rpm using Environ shaker thermostated at 35 ± 2 °C. The total hemoglobin (Hb) in the initial blood sample was measured using automatic hematology analyzer (Sysmex-K4500). The free Hb liberated into the plasma after exposure to the samples was estimated in each sample by measuring absorbance of diluted plasma with diode array spectrophotometer (HP 8453, Hewlett-Packard GmbH/Germany). Percentage of hemolysis was calculated from the following formula:

$$\%\,\text{Hemolysis} = \frac{\text{Free Hb}}{\text{Total Hb}} \times 100$$

Here reported value is the mean of three replicates.

3. Results and discussion

3.1. Synthesis and physicochemical characterization of Alg–Ccm AuNPs and MP@Alg–Ccm AuNPs

Among the nanotherapeutics, suitably functionalized AuNPs are widely used for drug delivery applications. Different types of reductants and capping agents have been used for the generation and stabilization of AuNPs with desired size and shape. Most of the studies describe multiple steps for the generation of drug conjugated polymer functionalized AuNPs. Besides, hazardous organic solvents are usually employed for conjugating hydrophobic drugs onto the surface of functionalized AuNPs. In this study water soluble curcumin conjugated biopolymer stabilized AuNPs were fabricated in a single step using Alg–Ccm conjugate and the Alg–Ccm AuNPs were further fabricated with another anticancer drug MTX to generate MP@Alg–Ccm AuNPs. Most interestingly, the dual drug conjugated polymer functionalized AuNPs were developed following a green synthetic route as depicted in Scheme 1 without using any hazardous organic solvent. We have recently developed the water soluble Alg–Ccm conjugate (Dey & Sreenivasan, 2014). AuNPs were generated using the aqueous solution of Alg–Ccm conjugate under thermal activation. Here alginate played the role of both reducing and stabilizing agent. In order to develop a dual drug delivery vehicle with improved targeting ability, antifolate drug MTX was also covalently conjugated to the Alg–Ccm AuNPs. MTX serves not only as a chemotherapeutic agent; being an analog of folic acid it also plays the role of a targeting ligand. In this study MTX was first conjugated to bis(aminopropyl) terminated PEG to produce MTX-PEG conjugate (MP conjugate; see the *inset* in Scheme 1) in aqueous buffer solution. The MP conjugate was eventually conjugated to Alg–Ccm AuNPs following EDC chemistry to generate MP@Alg–Ccm AuNPs (as shown in Scheme 1).

Generation and stabilization of AuNPs by Alg–Ccm conjugate was proved by the distinctive SPR absorption of Alg–Ccm AuNPs at ~ 525 nm (Fig. 1A). It is clear from Fig. 1A that the characteristic absorbance of curucmin (at around 427 nm in Alg–Ccm) was masked by the strong SPR band of Alg–Ccm AuNPs. However, the sharp peak at 280 nm evidently indicated the capping of AuNPs by Alg–Ccm conjugate. In Fig. 1B the X-ray diffractogram of both Alg–Ccm conjugate and Alg–Ccm AuNPs are shown. The X-ray diffractogram of the conjugate indicated almost amorphous or disordered crystalline phase. However, the XRD pattern of Alg–Ccm

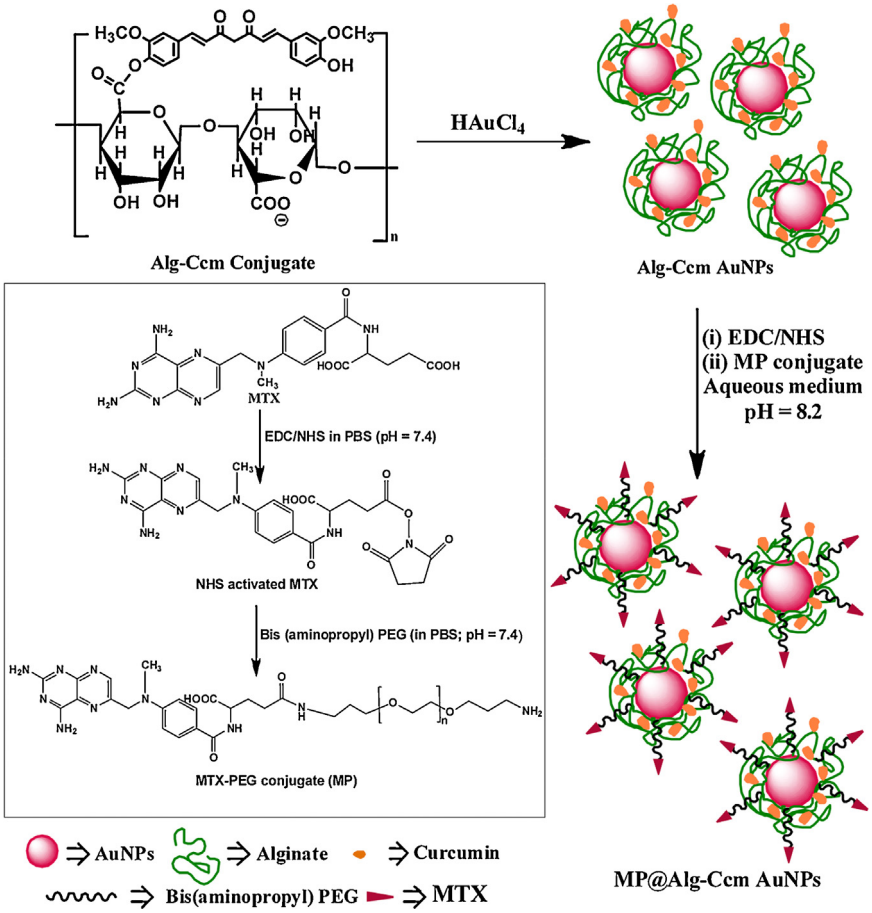

Scheme 1. Schematic presentation for the fabrication of MP@Alg–Ccm AuNPs *via* green route (*inset*: synthetic route to develop MP conjugate) (For interpretation of the references to colour in this scheme legend, the reader is referred to the web version of this article.).

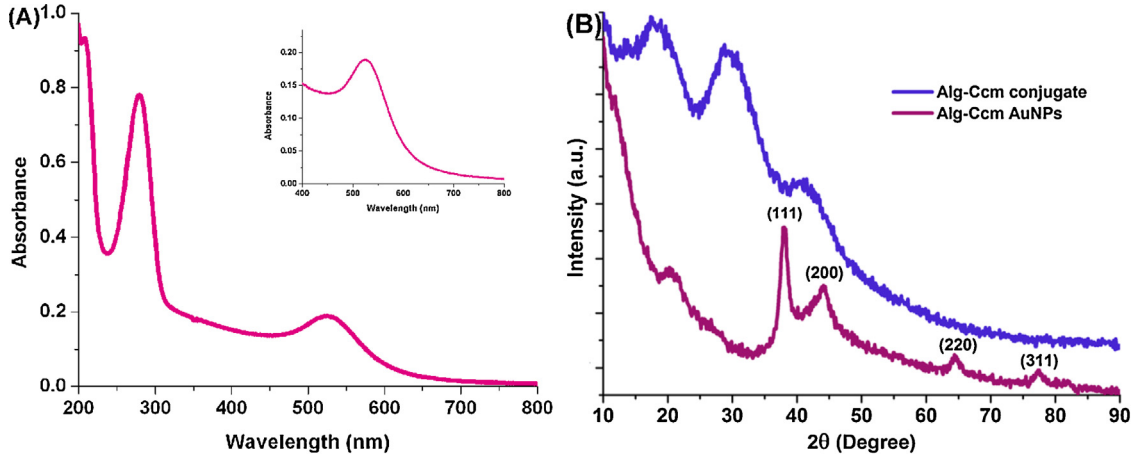

Fig. 1. (A) SPR absorption of Alg–Ccm AuNPs (*inset*: picture of the same in the visible range) and (B) XRD patterns of Alg–Ccm conjugate and Alg–Ccm AuNPs.

AuNPs showed distinct Bragg reflections corresponding to (1 1 1), (2 0 0), (2 2 0) and (3 1 1) Miller indices. Thus the diffractogram confirmed face centered cubic (FCC) crystalline geometry of the AuNPs formed using Alg–Ccm conjugate.

The formation of MP conjugate was confirmed by FTIR and UV–vis spectroscopic analyses and the results are detailed in the Supplementary Information (Fig. S1 and S2).

Shift in the SPR absorption of AuNPs is an indication of surface modification of the NPs (Liang et al., 2010). In MP@Alg–Ccm AuNPs the SPR band was red-shifted to 539 nm (Fig. 2). Chemical adsorption of MP conjugate onto the surface of Alg–Ccm AuNPs caused perturbation in the dielectric constant of the medium surrounding the NPs resulting in a red-shift of the SPR band. In the absorption spectrum of MP@Alg–Ccm AuNPs a distinct peak at around 369 nm (see the *inset* of Fig. 2) further indicated the presence of MTX in MP@Alg–Ccm AuNPs.

In order to thoroughly characterize the chemical structure of drug conjugated AuNPs, FTIR spectra of the AuNPs were recorded after each stage of modification. Fig. 3A and B represents the spectra of Alg–Ccm AuNPs and MP@Alg–Ccm AuNPs respectively. In Fig. 3A, the peak at 3437 cm^{-1} is assigned to the —OH stretching vibration and peaks at around 1650 cm^{-1} and 1647 cm^{-1} are attributed to the stretching vibration of —C=O functionality in Alg–Ccm AuNPs. According to our hypothesis, alginate reduced Au(III) to Au(0) and the —OH functional group of alginate was oxidized to —C=O functionality and this —C=O stretching vibration appeared as a small peak at around 1701 cm^{-1} (Fig. 3A). The small peak at 1211.2 cm^{-1} is due to the ester —C—O vibration in the conjugate. In the FTIR spectrum of MP@Alg–Ccm AuNPs (in Fig. 3B), the appearance of new peak at around 1409 cm^{-1} clearly indicates the presence of MTX and the new peak at 1550 cm^{-1} (due to combination of N—H stretch and N—H bending) supports the formation of amide linkage. Formation of both Alg–Ccm AuNPs and MP@Alg–Ccm AuNPs was confirmed by ^{1}H NMR spectra of both the systems as shown in Fig. 4.

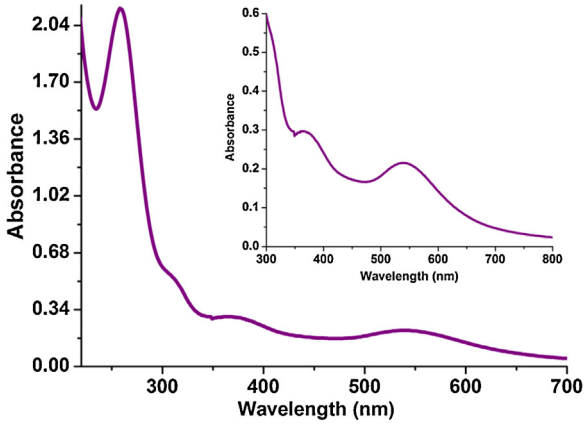

Fig. 2. SPR absorption of MP@Alg–Ccm AuNPs (*inset*: picture of the same from 300 to 800 nm range emphasizing the peak at 369 nm).

Fig. 4A shows the ^{1}H NMR spectrum of Alg–Ccm AuNPs in which the methine protons of hexuronic acid residues of alginate appeared at $\delta \approx 3.5$–5 ppm and the peaks at δ 6.9 and 7.9 are due to the aromatic protons of Ccm. However, the chemical shift due to the characteristic —OCH_3 protons of Ccm probably merged with the chemical shift of C-5 methine proton of mannuronic acid (M) unit of alginate ($\delta \approx 3.81$ ppm). In Fig. 4B, the multiple peaks at $\delta \approx 1.7$–3.8 ppm were observed due to the protons from bis(aminopropyl) terminated PEG unit. Some of the peaks merged with that of alginate protons. However, the peaks that appeared in the range of $\delta \approx 6.9$–8.7 ppm can be attributed to the aromatic protons of both Ccm and MTX.

The sizes and zeta potential values for the aqueous suspension of Alg–Ccm AuNPs and MP@Alg–Ccm AuNPs determined by DLS are tabulated in Table 1. The hydrodynamic diameter of MP@Alg–Ccm AuNPs being small enough (~187 nm), the DDS can be considered as a suitable candidate for entering into the cancer cells exploiting the EPR effect. Stability of Alg–Ccm AuNPs and MP@Alg–Ccm AuNPs in aqueous suspension was evaluated by the zeta potential measurement. The sufficiently high negative zeta potential ($\zeta = -39.5 \pm 0.02$ mV at pH 7.4 and 25 °C) for Alg–Ccm AuNPs indicates potential stability of the nano-system in aqueous medium. However, the ζ-potential value dropped to -25.8 ± 0.05 mV upon chemisorptions of MP conjugate onto the surface of Alg–Ccm AuNPs. This decrease in surface charge can be attributed to the presence of PEG chains (possessing stealth potential) onto the surface of MP@Alg–Ccm AuNPs (Manson, Kumar, Meenan, & Dixon, 2011). However; reduced negative surface charge was adequate to impart stability to the NPs as evident from the TEM images of the well-dispersed particles shown in Fig. 5.

Table 1
DLS data of Alg–Ccm AuNPs and MP@Alg–Ccm AuNPs.

Material	Hydrodynamic diameter (nm)	Zeta potential (ζ, mV)
Alg–Ccm AuNPs	132 ± 2 (PDI: 0.60)	−39.5 ± 0.02
MP@Alg–Ccm AuNPs	187 ± 4 (PDI: 0.43)	−25.8 ± 0.05

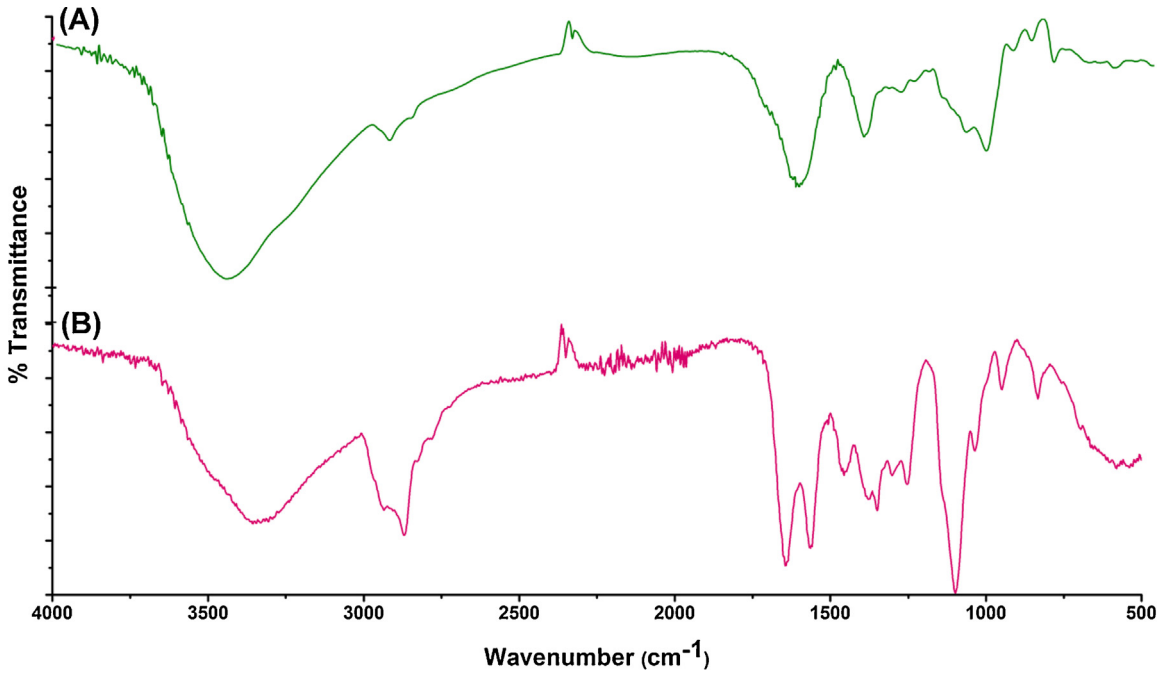

Fig. 3. FTIR spectra of (A) Alg–Ccm AuNPs and (B) MP@Alg–Ccm AuNPs.

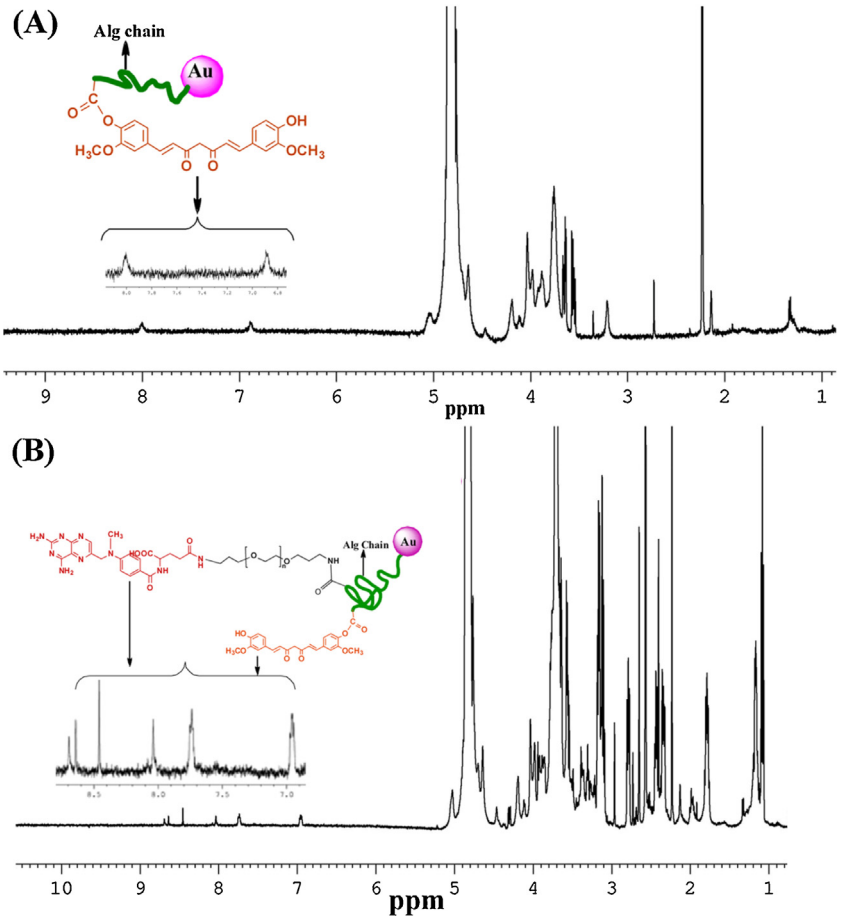

Fig. 4. ^{1}H NMR spectra of (A) Alg–Ccm AuNPs and (B) MP@Alg–Ccm AuNPs.

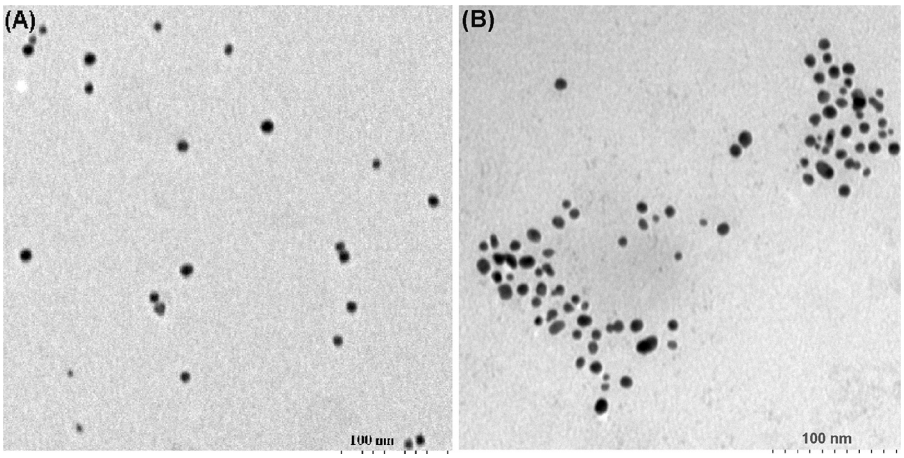

Fig. 5. TEM images of (A) Alg–Ccm AuNPs and (B) MP@Alg–Ccm AuNPs.

It is well studied that NPs with positive surface charge or hydrophobic exteriors are prone to plasma protein adsorption and hence are susceptible to reticuloendothelial system (RES) clearance. As here the negatively charged AuNPs are protected with hydrophilic, non-immunogenic biopolymer "alginate" and biocompatible polymer PEG, hence the particles might escape unwanted protein adsorption and RES clearance resulting in longevity in systemic circulation and enhanced EPR effect (Aryal, Grailer, Pilla, Steeberb, & Gong, 2009).

3.2. Drug content and cytotoxic potential of MP@Alg–Ccm AuNPs

From UV–vis spectroscopic study it was revealed that 100 mg of MP@Alg–Ccm AuNPs contained 1.05 ± 0.01 mg of Ccm and 1.26 ± 0.05 mg of MTX. In order to assess the cytotoxic potential of the double drug containing nano-vector, cell viability (%) was checked against C6 glioma and MCF-7 cancer cell lines after interaction with different concentration of MP@Alg–Ccm AuNPs and thereafter compared with that of each of the free drug of equivalent concentration.

Fig. 6 shows the cytotoxic activity of MP@Alg–Ccm AuNPs after interaction with the cancer cells in comparison with free drugs of equivalent concentrations. For each cell line, MP@Alg–Ccm AuNPs exhibited improved cytotoxicity compared to the individual drug (MTX/Ccm) at all tested concentrations. This observation can be attributed to several factors like the synergistic effect exerted by the co-administration of MTX and Ccm, pleiotropic effect of Ccm and improved uptake of the nano-sized drug delivery system (DDS) by cancer cells. Here it can be reasoned that as MTX was conjugated with bis(aminopropyl) terminated PEG and then conjugated with Alg–Ccm AuNPs, hence the efflux of the drug from cancer cells was probably reduced considerably resulting in improved cytotoxicity of the DDS than that of the equivalent concentrations of free drugs. Improvement in the internalization of the DDS may be expected due to the size in the nm scale and presence of MTX as one of the drug.

3.3. Cellular uptake study

The nano-sized DDS was easily uptaken by both C6 and MCF-7 cancer cells. The bright green intracellular fluorescence observed in both the cells indicated the facile uptake. MTX uptake is known to take place through at least two different carrier systems such as (i) the folate receptors (FR) and (ii) the reduced folate carriers (Kohler et al., 2005). Here both C6 and MCF-7 cells possess folate receptors and in addition, MCF-7 contains reduced folate carriers to which MTX has superior affinity than that of folate receptor (Trippett et al., 2001; Wang, Zhao, & Goldman, 2004). In Fig. 7(A)–(F) the bright green intracellular fluorescence from C6 and MCF-7 cells indicating potential uptake of the DDS by the cancer cells.

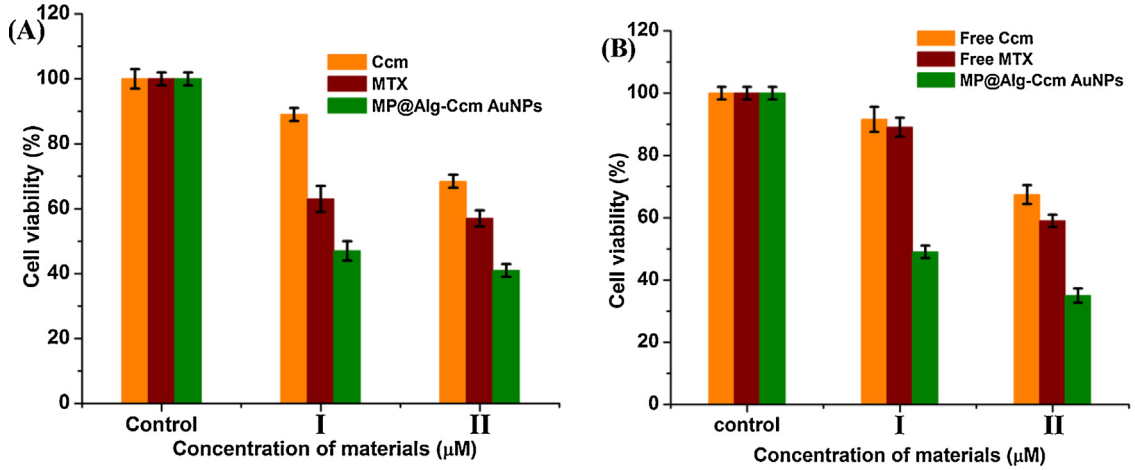

Fig. 6. Cell viability of (A) glioma cells and (B) MCF-7 cells after being exposed to different concentrations of MP@Alg–Ccm AuNPs in comparison with equivalent amount of free drugs, where I: 20.5 μM MTX + 21 μM Ccm in DDS & equivalent free drugs and II: 41 μM MTX + 42 μM Ccm in DDS & equivalent free drugs. The error bars indicate mean ± standard deviations and here $n = 3$.

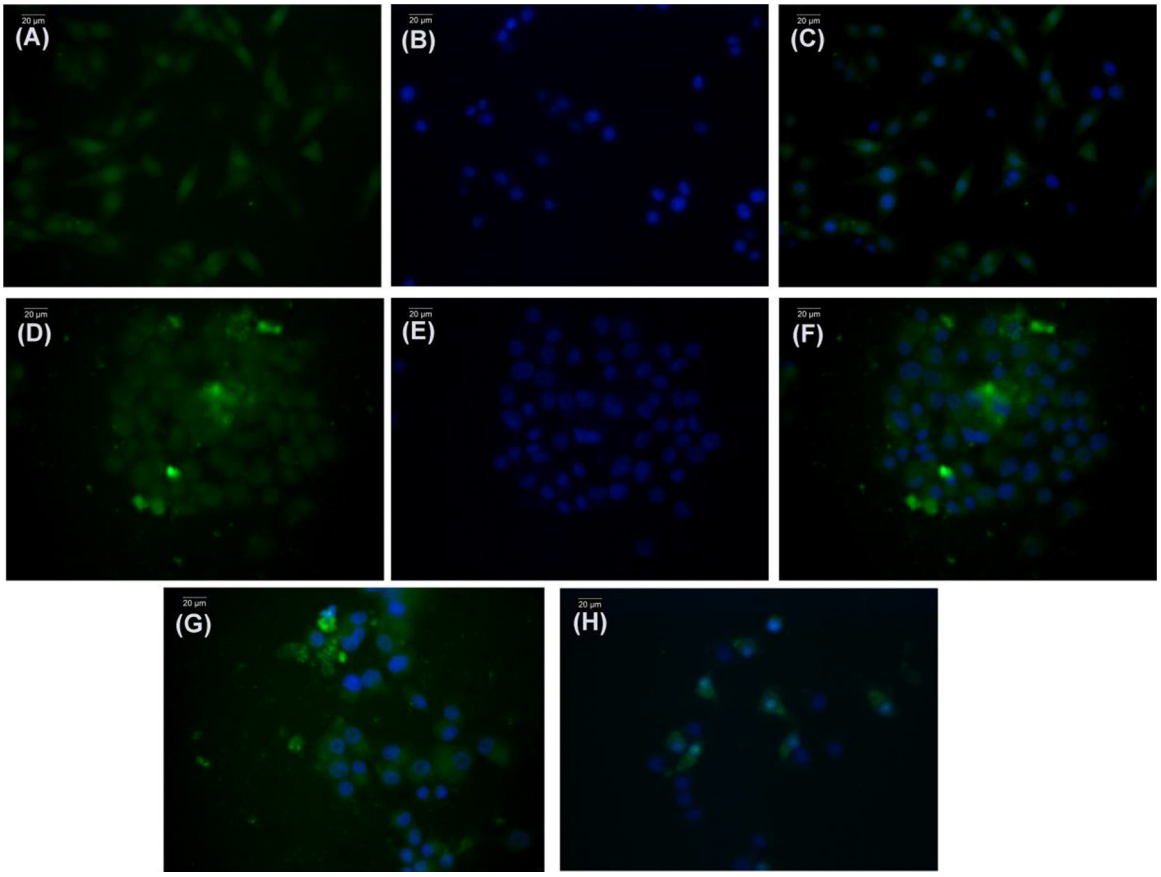

Fig. 7. Fluorescence microscopic images after incubation with FITC labeled MP@Alg–Ccm AuNPs for 3 h; glioma cells: (A) fluorescent image, (B) Hoechst 33342 stained nucleus and (C) merged fluorescent image; MCF-7 cells: (D) fluorescent image, (E) Hoechst 33342 stained nucleus and (F) merged fluorescent image; (G) and (H): merged fluorescent images of MCF-7 cells after being exposed to FITC labeled MP@Alg–Ccm AuNPs and FITC labeled Alg–Ccm AuNPs, respectively.

In a study by Chen et al. (2013), it has been shown by microscopic images that a multifunctional fluorescent nanogel based DDS was uptaken in a higher extent by FR positive MDA-MB-231 cells when it was decorated with FA and uptake was lower for the DDS without any FA decoration. Similarly in this study, MCF-7 cells were exposed to MP@Alg–Ccm AuNPs and Alg–Ccm AuNPs both of which was tagged with same density of FITC. Here MCF-7 cell line was chosen for this study as MTX has higher affinity to reduced folate carriers

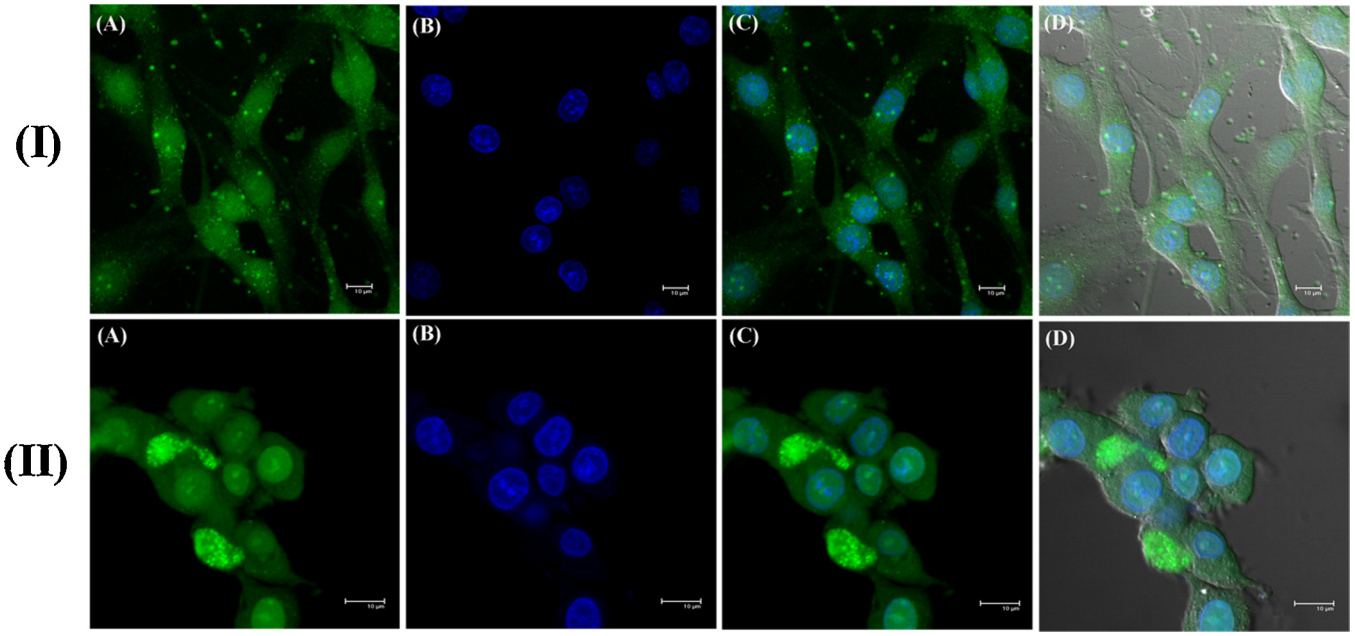

Fig. 8. Confocal laser scanning microscopic images after incubation with FITC labeled MP@Alg–Ccm AuNPs for 3 h; (I) C6 glioma cells and (II) MCF-7 cells: (A) fluorescent image, (B) Hoechst 33342 stained nucleus, (C) merged fluorescent image in dark field and (D) merged fluorescent image in bright field.

that are over expressed in MCF-7 cells. Comparing the merged fluorescent images in Fig. 7G and H, it was qualitatively confirmed that improved uptake of MP@Alg–Ccm AuNPs by MCF-7 cells was due to the targeting efficiency of MTX.

In addition, internalization of MP@Alg-Ccm AuNPs was further confirmed by recording confocal laser scanning microscopic (CLSM) images as depicted in Fig. 8. Fig. 8(I) shows the CLSM images of C6 glioma cells and Fig. 8(II) shows the CLSM images of MCF-7 cells after internalization of FITC tagged MP@Alg–Ccm AuNPs utilizing the green fluorescence of FITC and the nucleus of the cells were stained with Hoechst 33342.

3.4. Evaluation of hemolytic toxicity

In order to evaluate the hemolytic toxicity of MP@Alg–Ccm AuNPs, the % hemolysis caused by the DDS was determined. It was found that for a concentration of 0.5 mg/mL the hemolysis was $0.11 \pm 0.001\%$ which was much less than the acceptable limit of 5%. Hence the DDS was found to be safe for intravenous administration. Here it can be reasoned that, though the DDS contained two cytotoxic drugs but the presence of non-immunogenic biopolymer "alginate" and biocompatible "PEG" on the surface of the AuNPs made the DDS hemocompatible in nature.

4. Conclusions

In conclusion, we have developed a dual drug conjugated, biopolymer stabilized, targeted DDS based on AuNPs. In this study, at first Ccm conjugated AuNPs were fabricated using Alg–Ccm conjugate in aqueous medium under thermal activation. Alginate, the "green chemical", reduced Au(III) to Au(0) and simultaneously stabilized the nascent AuNPs. A MTX conjugate of bis(aminopropyl) terminated PEG was also developed and the MP conjugate was further conjugated to Alg–Ccm AuNPs to develop the MTX and Ccm conjugated DDS. Thus, dual drug conjugated AuNPs were fabricated using two facile reaction steps and employing "green solvent" water. Thus this study is interesting from the synthetic point of view. In addition, the targeted DDS exhibited improved cytotoxicity compared to each of the free drugs of equivalent concentration. Synergistic effect of two anti-neoplastic agents, pleiotropic effect of Ccm and improved uptake due to targeting efficiency of MTX probably played the major role to result in superior cytotoxic effect of MP@Alg–Ccm AuNPs. Facile uptake of the hybrid nano-structured DDS by cancer cells was confirmed by both fluorescence microscopic and confocal laser scanning microscopic imaging. The DDS was also found to be hemocompatible in nature. Development of multi drug resistance (MDR) is the major barrier to successful chemotherapeutic treatment of cancer and coadministration of more than one chemotherapeutic agent (*i.e.* combination chemotherapy) can tame MDR to a large extent. Thus the DDS illustrated here can be developed further for the potential application in targeted combination chemotherapy to treat cancer.

Acknowledgements

The authors gratefully acknowledge the financial assistance provided by CSIR, New Delhi, India to conduct the study. The authors also thank Director and Head, SCTIMST, Trivandrum for providing the facilities.

Appendix A. Supplementary data

Supplementary data associated with this article can be found, in the online version, at doi:10.1016/j.carbpol.2015.09.016.

References

Aggarwal, B. B., Kumar, A., & Bharti, A. C. (2003). Anticancer potential of curcumin: Preclinical and clinical studies. *Anticancer Research*, *23*, 363–398.
Aggarwal, B. B., & Sung, B. (2009). Pharmacological basis for the role of curcumin in chronic diseases: An age-old spice with modern targets. *Trends in Pharmacological Sciences*, *30*, 85–94.
Anand, P., Kunnumakkara, A. B., Newman, R. A., & Aggarwal, B. B. (2007). Bioavailability of curcumin: Problems and Promises. *Molecular Pharmaceutics*, *4*, 807–818.
Aryal, S., Grailer, J. J., Pilla, S., Steeberb, D. A., & Gong, S. (2009). Doxorubicin conjugated gold nanoparticles as water-soluble and pH-responsive anticancer drug nanocarriers. *Journal of Materials Chemistry*, *19*, 7879–7884.
Boisselier, E., & Astruc, D. (2009). Gold nanoparticles in nanomedicine: Preparations, imaging, diagnostics, therapies and toxicity. *Chemical Society Reviews*, *38*, 1759–1782.
Bouhadir, K. H., Hausman, D. S., & Mooney, D. J. (1999). Synthesis of cross-linked poly(aldehyde guluronate) hydrogels. *Polymer*, *40*, 3575–3584.
Chen, Y., Wilbon, P. A., Zhou, J., Nagarkatti, M., Wang, C., Chu, F., et al. (2013). Multifunctional self-fluorescent polymer nanogels for label-free imaging and drug delivery. *Chemical Communications*, *49*, 297–299.
Daniel, M. C., & Astruc, D. (2004). Gold nanoparticles: Assembly, supramolecular chemistry, quantum-size-related properties, and applications toward biology, catalysis, and nanotechnology. *Chemical Reviews*, *104*, 293–346.
Dey, S., & Sreenivasan, K. (2014). Conjugation of curcumin onto alginate enhances aqueous solubility and stability of curcumin. *Carbohydrate Polymer*, *99*, 499–507.
Dhanasekaran, S., Biswal, B. K., Sumantran, V. N., & Verma, R. S. (2013). Augmented sensitivity to methotrexate by curcumin induced overexpression of folate receptor in KG-1 cells. *Biochimie*, *95*, 1567–1573.
Dhar, S., Liu, Z., Thomale, J., Dai, H., & Lippard, S. (2008). Targeted single-wall carbon nanotube-mediated Pt(IV) prodrug delivery using folate as a homing device. *Journal of American Chemical Society*, *130*, 11467–11476.
Duan, J., Mansour, H. M., Zhang, Y., Deng, X., Chen, Y., Wang, J., et al. (2012). Reversion of multidrug resistance by co-encapsulation of doxorubicin and curcumin in chitosan/poly(butyl cyanoacrylate) nanoparticles. *International Journal of Pharmaceutics*, *426*, 193–201.
Ganta, S., & Amiji, M. (2009). Coadministration of paclitaxel and curcumin in nanoemulsion formulations to overcome multidrug resistance in tumor cells. *Molecular Pharmaceutics*, *6*, 928–939.
Giljohann, D. A., Seferos, D. S., Daniel, W. L., Massich, M. D., Patel, P. C., & Mirkin, C. A. (2010). Gold nanoparticles for biology and medicine. *Angewandte Chemie International Edition*, *49*, 3280–3295.
Gref, R., Minamitake, Y., Peracchia, M. T., Trubetskoy, V., Torchilin, V., & Langer, R. (1994). Biodegradable long-circulating polymeric nanospheres. *Science*, *263*, 1600–1603.
Kohler, N., Sun, C., Wang, J., & Zhang, M. (2005). Methotrexate-modified superparamagnetic nanoparticles and their intracellular uptake into human cancer cells. *Langmuir*, *21*, 8858–8864.
Lantz, R. C., Chen, G. J., Solyom, A. M., Jolad, S. D., & Timmermann, B. N. (2005). The effect of turmeric extracts on inflammatory mediator production. *Phytomedicine*, *12*, 445–452.
Larson, N., & Ghandehari, H. (2012). Polymeric conjugates for drug delivery. *Chemistry of Materials*, *24*, 840–853.
Liang, M., Lin, I. C., Whittaker, M. R., Minchin, R. F., Monteiro, M. J., & Toth, I. (2010). Cellular uptake of densely packed polymer coatings on gold nanoparticles. *ACS Nano*, *4*, 403–413.
Maeda, H., Wu, J., Sawa, T., Matsumura, Y., & Hori, K. (2000). Tumor vascular permeability and the EPR effect in macromolecular therapeutics: A review. *Journal of Controlled Release*, *65*, 271–284.
Maher, D. M., Bell, M. C., O'Donnell, E. A., Gupta, B. K., Jaggi, M., & Chauhan, S. C. (2011). Curcumin suppresses human papillomavirus oncoproteins, restores p53, rb, and ptpn13 proteins and inhibits benzo[a]pyrene-induced upregulation of HPV E7. *Molecular Carcinogenesis*, *50*, 47–57.
Malam, Y., Loizidou, M., & Seifalian, A. M. (2009). Liposomes and nanoparticles: Nanosized vehicles for drug delivery in cancer. *Trends in Pharmacological Science*, *30*, 592–599.
Manju, S., Sharma, C. P., & Sreenivasan, K. (2011). Targeted coadministration of sparingly soluble paclitaxel and curcumin into cancer cells by surface engineered magnetic nanoparticles. *Journal of Material Chemistry*, *21*, 15708–15717.
Manju, S., & Sreenivasan, K. (2012). Gold nanoparticles generated and stabilized by water soluble curcumin–polymer conjugate: Blood compatibility evaluation and targeted drug delivery onto cancer cells. *Journal of Colloid and Interface Science*, *368*, 144–151.
Manson, J., Kumar, D., Meenan, B. J., & Dixon, D. (2011). Polyethylene glycol functionalized gold nanoparticles: the influence of capping density on stability in various media. *Gold Bulletin*, *44*, 99–105.
Misra, R., & Sahoo, S. K. (2011). Coformulation of doxorubicin and curcumin in poly(d,l-lactide-*co*-glycolide) nanoparticles suppresses the development of multidrug resistance in K562 cells. *Molecular Pharmaceutics*, *8*, 852–866.
Moorthi, C., Manavalan, R., & Kathiresan, K. (2011). Nanotherapeutics to overcome conventional cancer chemotherapy limitations. *Journal of Pharmacy and Pharmaceutical Sciences*, *14*, 67–77.
Motterlini, R., Foresti, R., Bassi, R., & Green, C. J. (2000). Curcumin, an antioxidant and anti-inflammatory agent, induces heme oxygenase-1 and protects

endothelial cells against oxidative stress. *Free Radical Biology and Medicine*, *28*, 1303–1312.

Piper, J. R., McCaleb, G. S., & Montgomery, J. A. (1983). A synthetic approach to poly(.gamma.-glutamyl) conjugates of methotrexate. *Journal of Medicinal Chemistry*, *26*, 291–294.

Ravindran, J., Prasad, S., & Aggarwal, B. B. (2009). Curcumin and cancer cells: How many ways can curry kill tumor cells selectively? *American Association of Pharmaceutical Scientists Journal*, *11*, 495–510.

Riebeseel, K., Biedermann, E., Loser, R., Breiter, N., Hanselmann, R., Mulhaupt, R., et al. (2002). Polyethylene glycol conjugates of methotrexate varying in their molecular weight from MW 750 to MW 40000 synthesis characterization, and structure–activity relationships in vitro and in vivo. *Bioconjugate Chemistry*, *13*, 773–785.

Shi, M. X., Cai, Q. F., Yao, L. M., Mao, Y. B., Ming, Y. L., & Ouyang, G. L. (2006). Antiproliferation and apoptosis induced by curcumin in human ovarian cancer cells. *Cell Biology International*, *30*, 221–226.

Trippett, T. M., Garcia, S., Manova, K., Mody, R., Cohen-Gould, L., Flintoff, W., et al. (2001). Localization of a human reduced folate carrier protein in the mitochondrial as well as the cell membrane of leukemia cells. *Cancer Research*, *61*, 1941–1947.

Wang, Y., Zhao, R., & Goldman, I. D. (2004). Characterization of a folate transporter in HeLa cells with a low pH optimum and high affinity for pemetrexed distinct from the reduced folate carrier. *Clinical Cancer Research*, *10*, 6256–6264.

Yang, J. S., Ren, H. B., & Xie, Y. J. (2011). Synthesis of amidic alginate derivatives and their application in microencapsulation of λ-cyhalothrin. *Biomacromolecules*, *12*, 2982–2987.